Title

Multispectral fluorescence lifetime imaging device with a silicon avalanche photodetector.

Journal

Optics Express, 29(13)

ISSN

1094-4087

Authors

Zhou, Xiangnan

Bec, Julien

Yankelevich, Diego

et al.

Publication Date

2021-06-21

DOI

10.1364/oe.425632

Research Article | Vol. 29, No. 13 / 21 June 2021 / Optics Express 20105
Optics EXPRESS

Multispectral fluorescence lifetime imaging device with a silicon avalanche photodetector

XIANGNAN ZHOU,[1] JULIEN BEC,[1] DIEGO YANKELEVICH,[2] AND LAURA MARCU[1,*]

[1]*Department of Biomedical Engineering, University of California, 451 Health Sciences Drive, Davis, California 95616, USA*
[2]*Department of Electrical and Computer Engineering, University of California, 3101 Kemper Hall, Davis, California 95616, USA*
[*]*lmarcu@ucdavis.edu*

Abstract: We report the design, development, and characterization of a novel multi-spectral fluorescence lifetime measurement device incorporating solid-state detectors and automated gain control. For every excitation pulse (~1 μJ, 600 ps), this device records complete fluorescence decay from multiple spectral channels simultaneously within microseconds, using a dedicated UV enhanced avalanche photodetector and analog to digital convert (2.5 GS/s) in each channel. Fast (<2 ms) channel-wise dynamic range adjustment maximizes the signal-to-noise ratio. Fluorophores with known lifetime ranging from 0.5–6.0 ns were used to demonstrate the device accuracy. Current results show the clear benefits of this device compared to existing devices employing microchannel-plate photomultiplier tubes. This is demonstrated by 5-fold reduction of lifetime measurement variability in identical conditions, independent gain adjustment in each spectral band, and 4-times faster imaging speed. The use of solid-state detectors will also facilitate future improved performance and miniaturization of the instrument.

1. Introduction

Various label-free fluorescence spectroscopy and imaging techniques have been identified as a promising means for quantitative and sensitive investigation of changes in the biochemical composition of tissue both *in vivo* and *in vitro* [1]. Spectrally-resolved lifetime measurements, in particular, are of interest as the tissue autofluorescence originates from numerous endogenous constituents (e.g. structural proteins, metabolic enzyme co-factors, porphyrins, lipids and lipoproteins) with complex photo-physical properties and overlapping spectral emission [2]. Thus, lifetime measurements can improve the specificity of the fluorescence acquisition by resolving the decay dynamics of such fluorophores in multiple spectral bands [3]. Also, lifetime measurements are more robust when compared to spectral intensities. The latter are typically hampered by non-uniform tissue illumination, changes in fluorescence excitation-collection geometries, or presence of endogenous absorbers (e.g., blood) resulting in light intensity attenuation. Moreover, an instrument capable of measuring decay dynamics of tissue autofluorescence simultaneously in multiple spectral emission can generate a wealth of orthogonal parameters for a more complete assessment of tissue characteristics and underlying biochemical features as well as for superior tissue classification [4,5].

The most common implementation of fluorescence lifetime measurement is time correlated single photon counting (TCSPC), frequently used in microscopy. In TCSPC, tissue sample is excited by a high repetition rate laser and the fluorescence emission is detected by single photon photodetector(s) [6] including multichannel detectors such as multi-anode photomultipliers (PMT) [7,8] or Single Photon Avalanche Diode (SPAD) arrays [9]. TCSPC is well suited for microscopy because the low pulse energy excitation beam can be tightly focused onto tissue sample without causing significant thermal damage. However, detection of individual photons

#425632 https://doi.org/10.1364/OE.425632
Journal © 2021 Received 24 Mar 2021; revised 26 May 2021; accepted 28 May 2021; published 11 Jun 2021

Optics EXPRESS

necessitates that background light is kept to a minimum. This limits the TCSPC's potential in clinical setting, in which elimination of ambient room light is either impossible or creates a major disruption in clinical workflow. As a result, to date few clinically compatible TCSPC-based systems have been used in clinical applications. The more recent adoption of synchronous external illumination could address this shortcoming and facilitate a more effective implementation of TCSPC technique [9,10] in clinics in the future.

An alternative approach is pulse sampling of fluorescence emission transient in which a large amount of fluorescence photons is generated by a short (sub-ns) and intense excitation pulse (~0.1-10 μJ) and detected by a high-bandwidth photodetector [11,12]. The resulting electrical transient signal is captured with a fast digitizer with a resolution of tens of picosecond allowing fast recording (~few microseconds) of fluorescence decays. The large number of fluorescence photons generated within nanosecond means that background illumination is unlikely to adversely impact fluorescence signal. In addition, since analog detection technique is utilized, low frequency signal of ambient light can be filtered. This approach was found best suited for mesoscopic imaging (submillimeter resolution) of large areas (>10mm) due to the high energy excitation pulses (~0.1-10 μJ).

Successful implementation of the pulse sampling approach has employed both avalanche photodiodes (APD) and PMT. Earlier non-spectral resolved devices using APD were successfully used for colorectal cancer diagnosis *in vivo* [13] demonstrating the clinical potential of pulse sampling scheme but the identification of specific biochemical species was limited by the inability of the system to spectrally resolve the fluorescence emission . Later spectrally resolved devices utilizing PMT and a monochromator [12] demonstrated the clinical application of multispectral pulse sampling technique in studies of atherosclerotic plaques and brain tumors *in vivo*. Furthermore, the pulse sampling technique has enabled the construction of an instrument capable of simultaneous measurements of fluorescence lifetime in multiple spectral emission bands suitable for tissue characterization [14].

Our group has reported the first implementation of a practical point-scanning system consisting of a fiber optic probe, a single Microchannel Plate Photomultiplier Tube (MCP-PMT) detector, fast digitizer (12.5 GS/s) and temporal multiplexing scheme using different length of fiber optic delay lines for each spectral band of the instrument [15]. This instrument was further refined by our laboratory enabling fast system dynamic range adjustment [16], real-time data processing and real-time augmentation of fluorescence parameters for intraoperative tissue diagnosis and surgical guidance [17]. It is currently being evaluated in clinical settings to assess various tissue pathologies including oropharyngeal cancer [18] and brain tumors [19]. Also, it has been used extensively in benchtop experiments to investigate features of atherosclerotic lesions [20] and osteoarthritis [21], to identify positive cancer margins in breast tissue specimens [22], and to answer fundamental biomedical questions in tissue engineering [23,24]. The same time-multiplexing single PMT approach was adopted by others groups [25–27] and combined with galvanometer scanners for both *in vitro* and *in vivo* tissue diagnosis with a handhold endoscope [28] or scanning microscopy [25,29]. A limitation of this temporal multiplexing scheme stem from the use of a single MCP-PMT detector. The short delay between the arrival time of each channel (~50 ns) prevents adjustment of bias voltages for each individual channel. The detector gain must therefore be reduced to avoid saturation of the higher intensity channel, thus negatively impacting the signal-to-noise ratio (SNR) of the remaining channels.

In this article, we report the design, development, and performance evaluation of a pulse sampling Fluorescence Lifetime Imaging (FLIm) device using a multi-APDs scheme for simultaneous measurement of fluorescence lifetimes in multiple spectral channels addressing the limitations of existing configurations. In contrast to the earlier implementation using one MCP-PMT, the instrument reported here relies on dedicated solid-state silicon avalanche photodiodes (APDs) and gain modulation for each spectral channel. This configuration allows for optimization of

Optics EXPRESS

detection sensitivity in each spectral channel. While here we demonstrated a 3-channel detection scheme, this approach can be easily extended to a higher channel count, as needed. This new multispectral FLIm system is compact and suitable for tissue characterization and diagnosis in clinical environments.

2. Materials and methods

2.1. Overview of the device using APDs for simultaneous measurements of fluorescence lifetime in 3-spectral channels

The diagram of the APD-based multispectral FLIm device design is illustrated in Fig. 1. A pulsed 355 nm UV laser is used for fluorescence excitation (STV-02E-140, TEEM photonics, France). Excitation light is delivered to the sample by a fiber optic probe connected to the fiber probe port. The fiber probe consists of one multimode optical fiber (365 µm core diameter, 0.22 NA, FG365UEC, Thorlabs, USA). Fluorescence signal from the sample is collected using the same fiber probe, spectrally resolved by a set of dichroic mirrors and bandpass filters and directed to three variable gain UV enhanced Si APD module with integrated transimpedance amplifier. The device also includes a 440 nm laser (TECBL-50G-440-USB-TTL, Worldstartech, Canada) that serves as aiming beam enabling real-time visualization of location from where the fluorescence (point-measurement) is collected [30]. The entire optical system (except digitizer and computer) fits within a dimension of 25 cm x 21 cm. Two 2 channel digitizers with 1.5 GHz bandwidth and 2.5 GS/s per channel (NI PXIe-5162 digitizer National Instruments, Austin, Texas) were used for signal recording (not shown).

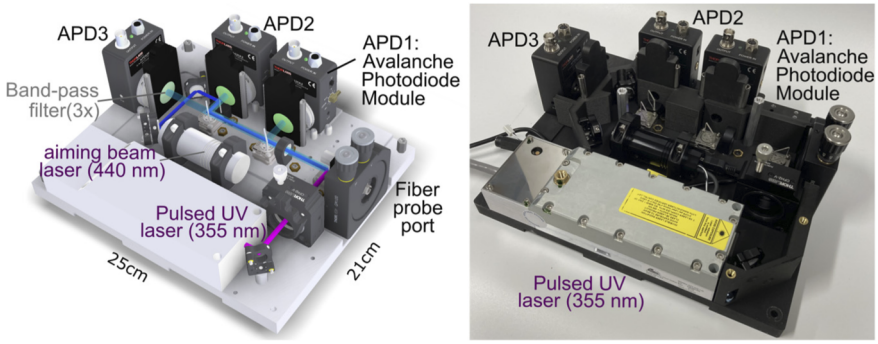

Fig. 1. Schematics and picture of the 3 channel APD-based fluorescence lifetime device.

2.2. APD module

The variable gain UV enhanced Si APD detector module was adapted from a commercially available module (APD430A2-SP1, Thorlabs, NJ) and consists of three main parts: 1) the APD detector 2) the post-detection amplifier circuit with fixed trans-impedance gain. 3) the analog control circuit adjusting the bias voltage of the APD detector, and hence the overall gain of the APD module. Table 1 lists the APD module characteristics. Figure 2(a) depicts a typical responsivity curve. The multiplication factor was measured for each APD modules (Fig. 2(b)).

The bias voltage control circuit modulates the bias voltage at the APD detector based on a control voltage. The accuracy, stability and response speed of the bias voltage control circuit directly determine the performance of the imaging system. As a result, the integrated bias voltage control circuit was designed based on the following characteristics: (1) The full gain (M=1-100) range of the APD module, corresponding to a maximum bias voltage of approximately 150 V at the APD detector was controlled by a 0-4.6 V control voltage. (2) The relationship between

Optics EXPRESS

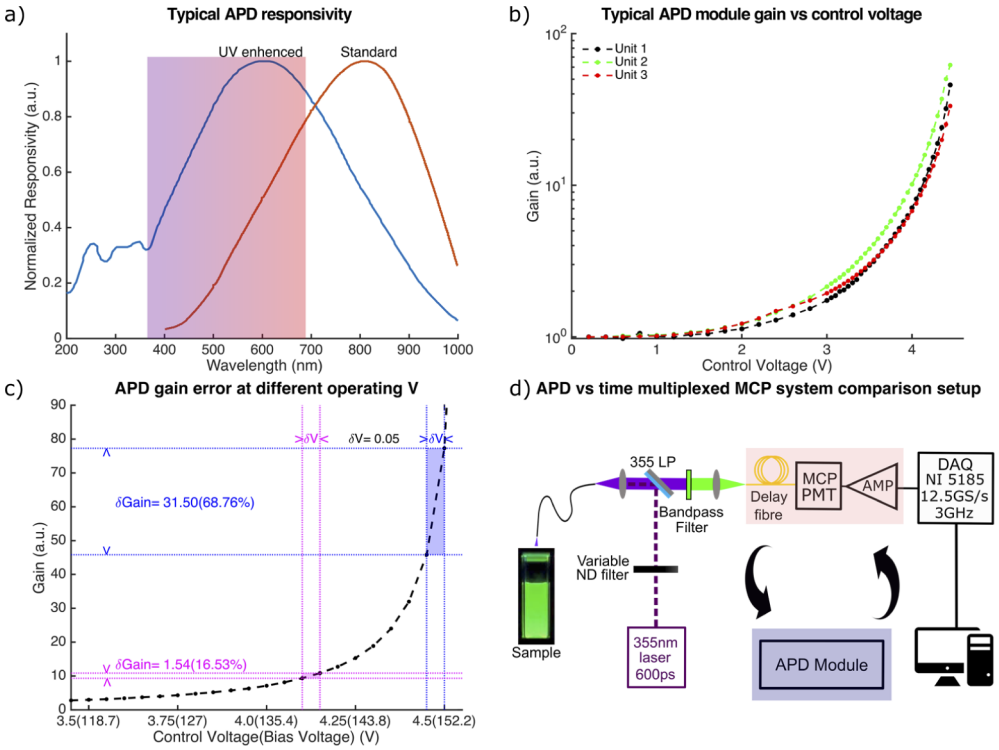

Fig. 2. a) Spectral response of UV enhanced APD and non-UV enhanced APD module. Shaded rainbow area represents the typical emission spectrum range of biological tissue excited by 355 nm laser. Adapted with permission from Thorlabs. b) Typical gain (multiplication factor) curve of the 3 APD modules. Unit-to-unit variation of the gain is observed. c) Due to APD modules' nonlinear behavior, same error in bias voltage leads to drastic different error of gain at different operating voltage. d) Schematics of the multi-APDs device vs time multiplexing MCP device used in the SNR comparison experiment.

Table 1. APD Module Specifications

Detector Type	UV Enhanced Silicon APD
Wavelength Range	200 - 1000 nm
Output Bandwidth (3 dB)	DC-400MHz
Active Area Diameter	0.2 mm
M Factor Adjustment Range	1 - 100 (Continuous)
Transimpedance Gain	5 kV/A (50 Ω Termination)
Max Conversion Gain	5.0×10^5 V/W

Optics EXPRESS

bias voltage (control voltage) and APD module gain was nonlinear (Fig. 2(b)), with unwanted variations of bias voltage leading to higher gain changes near the breakdown voltage (Fig. 2(c)). The bias voltage stability at 150 V should be such that a gain variation no greater than 2% is observed. (3) The speed of gain adjustment of the APD module determines the ability to accommodate rapid changes in fluorescence intensity. Thus, the bias voltage control circuit was designed to have a transit time of less than 2 ms which enables gain modulation at the laser repetition rate (< 500 Hz).

2.3. Optical throughput evaluation

To evaluate the ability to couple light from the fiber probe (365 µm core) onto APD detector sensitive area (200 µm diameter), a lens (A397TM-A, f=11 mm, NA=0.3, Thorlabs, NJ) was used to collimate the light emerging from a 365 µm-core fiber and then a second lens (C610TME-A, f=4.00 mm, NA=0.60; Thorlabs) was used to focus the light through a 200 µm size pinhole. The latter is representative of the APD aperture. The transmission efficiency was derived from optical power measurements before and after the pinhole (PM100D, Thorlabs, S120VC, 200–1100 nm, 50 mW).

2.4. Linearity characterization

To evaluate the linearity of the detection system and its effect on the fluorescence lifetime values, measurements were performed for different levels of excitation intensity and detector gain. These include measurement of Coumarin 120 (Exciton Coumarin 440) by varying the excitation intensity while keeping APD gain constant (M = 75) and obtained signals with amplitudes from 0.2 V to 1.4 V in a step of 0.1V and measurements for different levels of APD gain while keeping the excitation intensity constant and obtained signals with the same amplitude range (0.2 V– 1.4 V in a step of 0.1V). In addition, we tested various combinations of excitation intensity and APD gain such that a fixed peak signal (1 V) was maintained. In all configurations, 1000 waveforms were recorded at 2.5 GS/s. The instrument response function (IRF) was measured experimentally as stated in Section 2.8 for each APD gain level and used for lifetime deconvolution at corresponding APD gain level.

2.5. Performance characterization with fluorescent dyes and biomolecules

To determine the device lifetime measurement accuracy and precision, measurements were performed in solutions of organic dyes (100 µM concentration) with well-known fluorescence lifetimes and emission spectrum: Coumarin 120 (Exciton Coumarin 440) in ethanol, Rhodamine 6G (Sigma, R4127) in water and Rose Bengal B (Sigma Aldrich CAS 11121-48-5) in ethanol. Their fluorescence emission was recorded in the 390/40 nm, 470/28 nm and 542/50 nm spectral band, respectively. Three main endogenous tissue fluorophores, i.e., the structure proteins collagen and elastin, and the enzyme cofactor NADH were used to determine the device's ability to analyze more complex fluorescence dynamics of these biomolecules. Waveforms were acquired from Type 1 collagen from bovine achilles tendon (Sigma Aldrich CAS 9007-34-5, dry powder), elastin from bovine neck ligament (Sigma Aldrich CAS 9007-58-5, dry powder), and 250 µM NADH (Sigma Aldrich CAS 606-68-8) solution prepared in 100 mM Mops buffer at pH 7. For each measurement, 1000 waveforms were acquired at 2.5 GS/s.

2.6. Comparative FLIm device performance: APD vs MCP-PMT detection schemes

The ability of the multi-APDs FLIm device reported here to perform accurate fluorescence lifetime measurement of biological samples was assessed in comparison with the time multiplexing single PMT FLIm system in which a high-speed MCP-PMT detector (R3809U-50, Hamamatsu, 45 ps FWHM) together with a high-speed amplifier (AM–1607–SMA, Miteq, 40 dB, 0.01-3000 MHz) were utilized. The single PMT FLIm system has been fully described in our earlier publications

Optics EXPRESS

[24]. The dynamic range of this earlier device could be adjusted by varying the bias voltage of the PMT detector to account for the rapid change of fluorescence intensity [16].

We performed measurements under identical experimental conditions on fluorescent dyes with both multi-APDs and single PMT devices. Based on knowledge derived from prior benchtop experiments [23] and clinical studies [17], we determined experimental conditions that replicate the amount of signal typically encountered in clinical and pre-clinical setting. For clinical applications such as imaging of the oral cavity epithelium, a 400 mV peak fluorescence signal value was typically obtained in channel 1 (390/40 nm) with an PMT bias voltage of 1900 V. For benchtop applications, such as monitoring of engineered construct recellularization, a 400 mV peak fluorescence signal was typically observed in channel 3 (542/50 nm) with a PMT bias voltage of 2200 V. A single channel APD prototype was used in this experiment as shown in Fig. 2(d). During the experiment, laser power and excitation collection geometry were set to obtain the desired signal (400 mV peak) using the time multiplexing single PMT system at the pre-determined high voltage bias. The delay fiber, the PMT, and the amplifier were then replaced by the APD module. A signal with 400 mV peak voltage (the same as time multiplexing single PMT system) was obtained by adjusting the control voltage of APD module. For comparison between both devices, waveforms (n=1000) and IRF from both systems were acquired at 12.5 GS/s (NI PXIe-5185, National Instruments, Austin, Texas).

We also evaluated the integrated noise of both detecting schemes (detector and amplifier). Using the same 12.5 GS/s digitizer, the dark noise was measured and the noise power spectrum was calculated [31]. The APD detector was set to maximum gain (~100) while the high voltage bias of the MCP-PMT was set to 2200V. Responsivity values from both detectors at a wavelength of 540 nm were used for calculation.

2.7. Gain control characterization

The detector gain as a function of control voltage was characterized for each of the three APD detector modules. Specifically, constant incident light was directed to the detector and the output was recorded while the control voltage was increased in steps from 0.05 V to 4.6 V (0.2V steps were used to control voltage from 0.05 V -3.0 V and 0.05 V steps from 3.0 V - 4.6V.

The response time of the gain control circuitry was evaluated by monitoring the change in signal intensity (area under the curve of the measured detector pulse) following a step change (3.7 V to 4.4 V) of control voltage corresponding to a ~5x gain variation.

2.8. Optical fiber fluorescence background removal

Background fluorescence from optical fiber probe is typically presented in the acquired spectroscopic/imaging data, an undesirable effect that can be a significant obstacle to the extraction of fluorescence lifetime from the acquired waveforms. A computational method based on the normalization (scaling) of the fiber probe background fluorescence signal was applied to remove the background signal from the acquired waveform prior to lifetime computation. An illustration of the background removal process is shown in Fig. 3.

Fluorescence background waveform is acquired by holding the fiber probe in air (pointing away from any object) and adjusting the detector gain such that a good background fluorescence SNR is achieved. The waveform is then normalized (scaled) based on the amount of fluorescence signal generated by the fiber probe which is a constant during an imaging session. The amount of fiber probe fluorescence signal is computed as the area under the curve (AUC) of the waveforms in the region prior to tissue fluorescence signal arrive as indicated by the red dotted lines. The background is then normalized (scaled) and subtracted from the data with the normalization (scaling) factor calculated as the ratio of the AUC of the raw and background waveform. As this method is based on the constant fluorescence signal generated by fiber probe fluorescence, no knowledge of the detector gain is required making it a fast and simple but robust method.

Optics EXPRESS

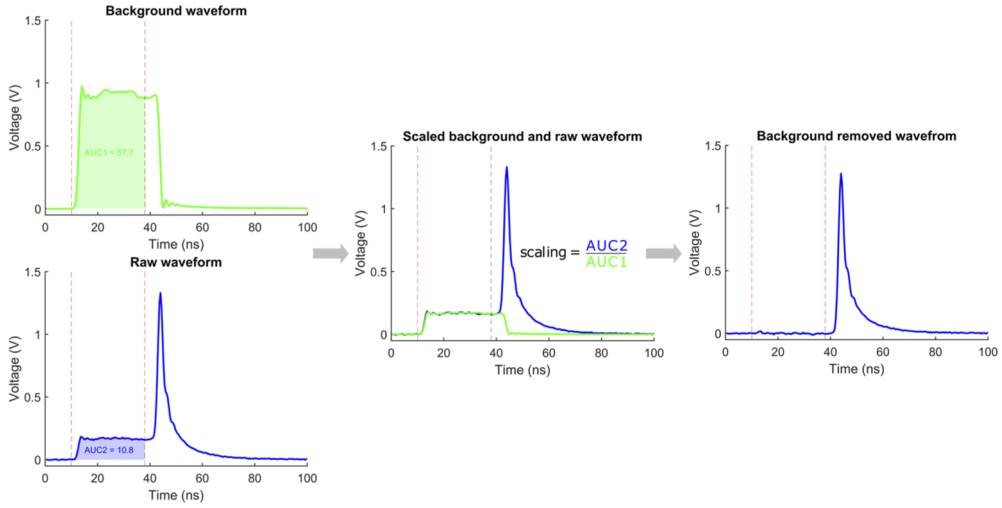

Fig. 3. Fluorescence background removal process. The background waveform is normalized (scaled) based on the fluorescence signal generated from the optical fiber probe, which should remain constant during image acquisition, and subtracted from the acquired raw waveform. The normalization (scaling) factor is computed as the ratio of area under the curve (AUC) between the red dotted lines of the raw waveform and background waveform. As the method is based on the constant signal of the fiber probe fluorescence, no knowledge of the detector gain is required making it a fast and simple but robust method.

2.9. Estimation of fluorescence lifetime values

Typically, three factors can lead to the broadening of the measured fluorescence emission waveform: 1) the duration of the excitation pulse, 2) the intermodal dispersion in the multimode optical fiber that results in broadening of the emitted light pulse, and 3) the response time of electronic components (detector and digitizer front end). To compensate for the fluorescence pulse distortion, the intrinsic fluorescence decay was recovered by numerical deconvolution of the instrument response function (IRF) from the measured fluorescence pulse transients.

The IRF in response to the 600 ps UV excitation pulse was measured using fluorescence pulses from two dye solutions. The 4-dimethylamino-4-cyanostilbene (DCS) (ChemBridge, San Diego, California) at 100 µM concentration in Cyclohexane was used to for 390/40 nm and 470/28 nm spectral channels. The hemicyanine dye 2-(p-dimethylaminosotyryl) pyridylmethyl iodide (2-DASPI) (Sigma-Aldrich, Cat. No. 280135) at 1 mM concentration in Ethanol was used for spectral channel of 542/50 nm. DCS dissolved in Cyclohexane has a very short (~66 ps) lifetime with fluorescence emission from 300nm - 500nm [6]. When dissolved in ethanol, 2-DASPI has a very short (~30 ps) average lifetime and an emission spectrum with a maximum at approximately 550 nm [32]. Unless otherwise stated, system IRF was acquired at 12.5 GS/s for PMT system and 5 GS/s for APD system.

For the APD-based device (except for data acquired for *Section 2.6 Comparative FLIm measurement of APD and MCP-PMT based devices*), the acquired fluorescence waveforms (sampled at 2.5 GS/s) were first re-sampled to 5 GS/s equivalent by interpolation prior to deconvolution to match the sampling rate of the system IRF. Lowpass interpolation algorithm 8.1 described in [33] implemented in MATLAB (MathWorks, Natick, Massachusetts) was used. This was necessary because the deconvolution algorithm requires the IRF and fluorescence to have identical sampling rates. To compensate for laser jitter, after re-sampling the fluorescence waveforms from all measurements were temporally aligned using a constant fraction discriminator

Optics EXPRESS

implemented in MATLAB (MathWorks, Natick, Massachusetts). This approach compares favorably to signal timing determination based on maximum waveform amplitude, adversely impacted by noise and limits in sampling rate, or leading-edge discriminator, subject to time walk when applied to waveforms of varying amplitudes [34,35]. An illustration of the data processing pipeline is shown in Fig. 4.

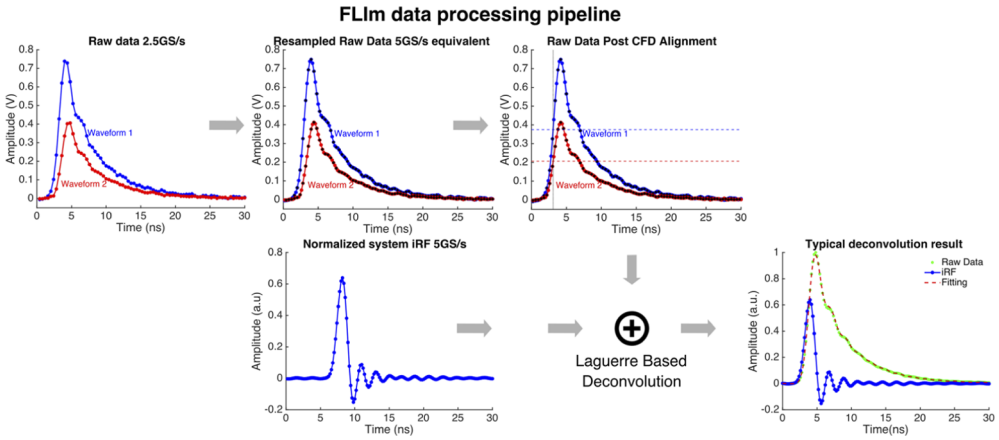

Fig. 4. FLIm signal processing pipeline. The raw signal acquired at 2.5 GS/s is first re-sampled to equivalent of 5 GS/s by interpolation to match the sampling rate of system IRF. After re-sampling the fluorescence waveforms from all measurements were temporally aligned using a constant fraction discriminator to compensate for laser jitter. The signal is then deconvolved using Laguerre expansion-based method to extract fluorescence lifetime and intensity. A fluorescence lifetime map can be generated for scanning application.

Signal deconvolution was performed using a fast algorithm (<10 µs per decay) previously reported by our group [36]. The algorithm is based on a constrained least-squares deconvolution with Laguerre expansion (CLSD-LE) method and has demonstrated robustness against noise.

2.10. Validation on tissue sample

To validate the performance of the multi-APD-based device and its ability to generate FLIm images, data was recorded by freehand scanning (2341 point measurements, ~35 cm^2 sample area, 70-second scanning duration) of a tissue sample (lamb) which presents a variety of tissue types (e.g., bone, bone marrow, fat, muscle and connective tissue) that enable direct visualization of fluorescence contrast. FLIm images were reconstructed from point measurements and their corresponding locations extracted from each frame (30 Hz) of a white light video of the specimen captured during the scanning by an external camera (CM3-U3-13Y3C-CS, Point Gray, with Fujinon HF9HA-1B 2/3"9 mm lens) [30]. FLIm measurement localization was achieved by a Convolutional Neural Network (CNN) based aiming beam localization algorithm [30]. Linear interpolation was used to determine the FLIm measurement location between each available video frames when high (480 Hz) laser repetition rate was used due to the limitation of camera frame rate (30 Hz).

To demonstrate the improved performance of the novel simultaneous multispectral APD FLIm system, two configurations of the 355 nm excitation laser were used: 1) 1 µJ per pulse at output of fiber probe, low (120 Hz) laser repetition rate (excitation parameters similar to the time-multiplexing multispectral PMT FLIm system currently used for clinical studies); 2) 0.25 µJ per pulse at output of fiber probe, high (480 Hz) laser repetition rate. Under both configurations, the UV exposure to tissue sample was identical and in compliance with IEC 60825 standard [37]. Four-fold averaging of acquired fluorescence waveforms was performed for both configurations.

Optics EXPRESS

3. Results

3.1. Optical throughput

The measured coupling efficiency of light transmitted from 365 µm multimode fiber through the 200 µm pinhole was found at 99%. This indicates a minimum effect of the small size of APD sensitive area on fluorescence photons collection efficiency.

3.2. System validation with fluorescent dyes and biomolecules

The computed lifetime values of the fluorescence dyes (Coumarin 120, Rhodamine 6G and Rose Bengal) and tissue fluorophores (collagen, elastin, and NADH) are listed in Table 2. These values were found in close agreement with those reported in the literature. Oscillation presented in the tail of fluorescence waveforms and system IRF (Fig. 4) did not pose any issue in the recovery of fluorescence lifetime values.

Table 2. Lifetime measurement and literature values for fluorescence dyes and tissue fluorophores used for system validation

		Measured		Literature
Fluorophore	Wavelength (nm)	Lifetime (ns)	Standard deviation (ns)	Lifetime (ns)
Rosxe Bengal in ethanol	390/40	0.834	0.080	0.850 [6]
Coumarin 120 in ethanol	470/28	3.60	0.034	3.64 [38]
Rhodamine 6G in H_2O	542/50	3.97	0.080	4.08 [39]
Collagen	390/40	5.621	0.093	3.49-5.30 [40]
NADH	470/28	0.472	0.039	0.30-0.50 [6]
Elastin	470/28	6.124	0.097	5.20-7.36 [41]

3.3. APD module temporal response dependency on APD gain and signal amplitude

Changes in measured fluorescence pulses waveforms (e.g., C120 dye) as a function of APD gain and excitation intensities are shown in Figs. 5(a) and (c), respectively. The normalized waveforms to peak intensity indicate that a decreased gain leads to a nonlinear behavior (Fig. 5(b), with most noticeable oscillations observed at the low gain (M=3). While the tail of the fluorescence pulse as well as the measured IRF shows noticeable oscillation, the numerical deconvolution algorithm accounts for this behavior as seen in Fig. 4.

The impact of APD gain and signal amplitude on the APD module temporal response (Fig. 5) may influence the ability to accurately estimate fluorescence lifetimes. This effect was systematically evaluated by reporting the distribution of computed lifetimes after deconvolution in each configuration (Fig. 6). Deconvolution was performed using a single IRF as well as using an IRF for each individual gain value (matching IRF). As seen in Fig. 6(a), variations of optical signal amplitude have minimum effect on average estimated lifetimes, in good agreement with literature value of 3.64-3.85 ns [38], although as expected, lower signal amplitude leads to higher lifetime value standard deviation. Measurements at low gain led to an overestimation of estimated lifetime (Figs. 6(b) and (c)), this issue was addressed by using different IRFs for each gain value. We observed that compensating decrease of optical signal intensity by an increase in APD gain led to accurate lifetime estimations provided that different IRFs were used for each gain (Fig. 6(c)). Interestingly, this did not lead to an increase in estimated lifetime standard deviation.

3.4. APD System SNR evaluation

The recovered fluorescence lifetime of the APD system (3.573 ± 0.061 ns) was found in good agreement with that of the MCP-PMT system (3.66 ± 0.291 ns). However, higher SNR was

Optics EXPRESS

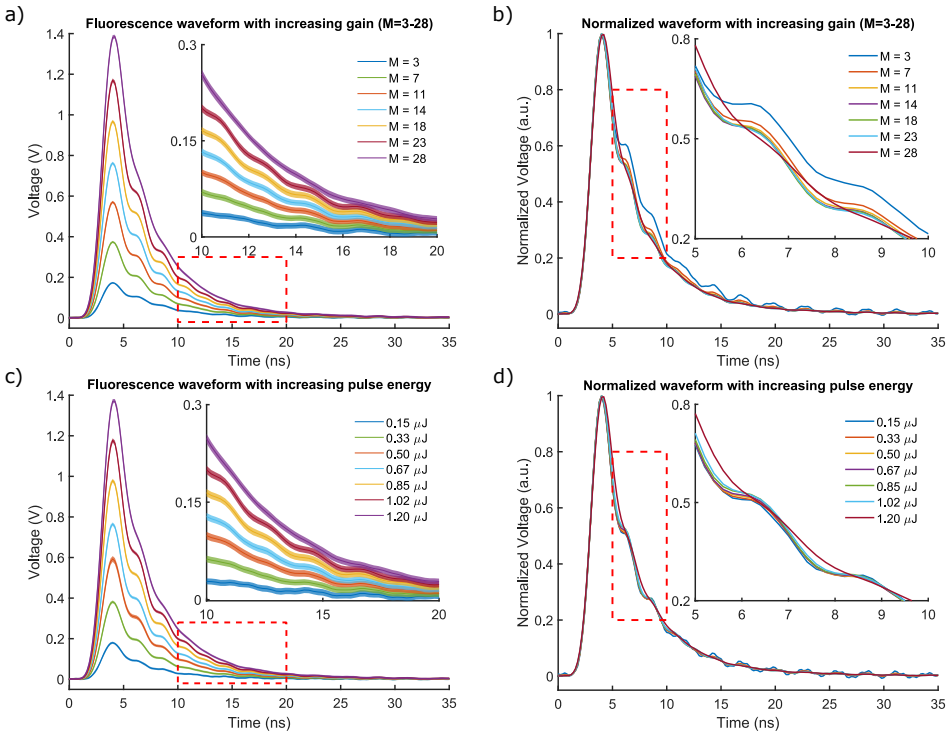

Fig. 5. Investigation of measured fluorescence waveforms as a function of signal amplitude and APD gain, characterized using 1000 measurements of Coumarin 120 solution. a) Mean and standard deviation of fluorescence waveforms at different APD gain. b) Display of normalized averaged waveforms highlights some difference of temporal response that may affect estimated lifetime. c) Mean and standard deviation of fluorescence waveforms at different optical signal intensity (obtained by varying the laser pulse energy). d) Display of normalized waveforms highlights some difference in temporal response.

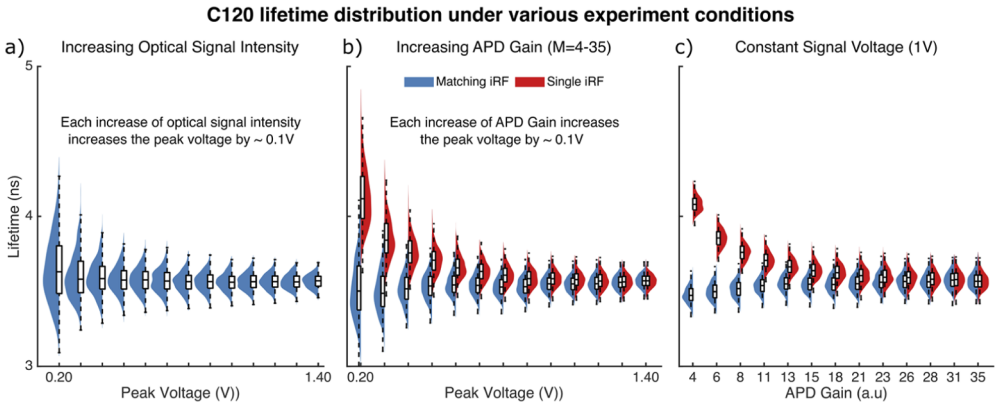

Fig. 6. Distribution of Coumarin 120 fluorescence lifetime under (a) increasing optical signal intensity. (b) increasing APD gain. (c) constant signal peak voltage (1 V) where each increase of APD gain is compensated by a decrease of optical signal intensity to maintain a constant 1 V peak voltage.

Optics EXPRESS

obtained with the APD-based system (Fig. 7(a)) compared to MCP-PMT system (Fig. 7(b)), resulting in 5-fold lower standard deviation of measured fluorescence lifetime.

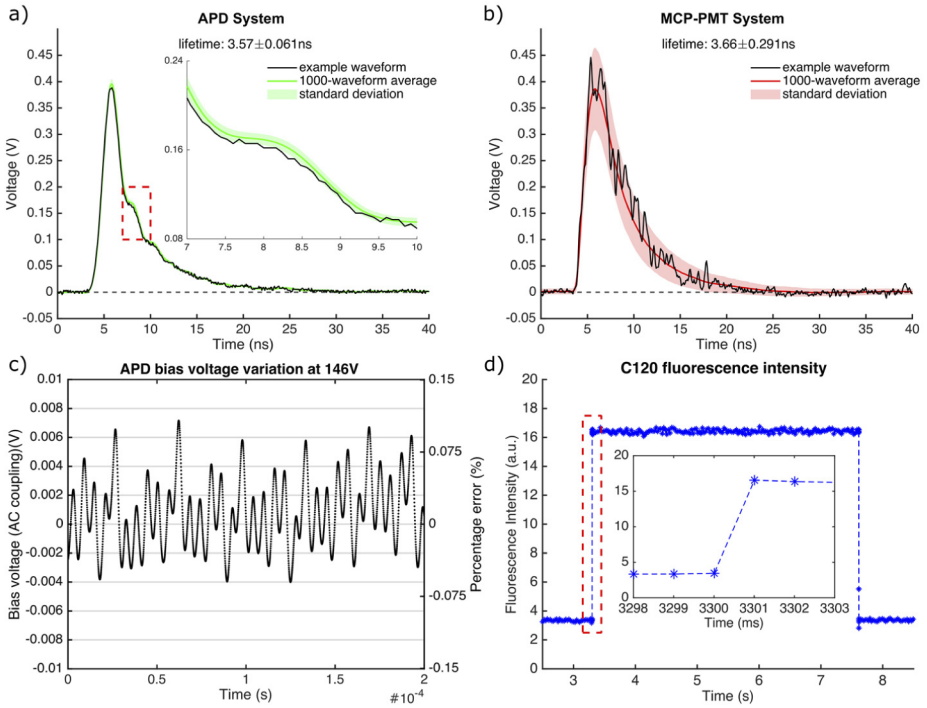

Fig. 7. Back-to-back SNR comparison of muti-APDs FLIm device (a) and time multiplexing single PMT FLIm device (b). Mean fluorescence waveform, one raw waveform and standard deviation (shaded area) were shown. c) Variation of APD bias voltage @146 V. Adapted with permission from Thorlabs. d) Response of the APD-based detection to a step change of bias voltage. The response time is less than 2 ms. No overshoot was detectable at either rising or falling edge. The time resolution of the measurement was 1 ms.

The integrated noise of the APD module (0–400 MHz) was measured as 4.06 nW, consistent with the value listed in the device data sheet, whereas the integrated noise of MCP-PMT and amplifier (0.01–3000 MHz) was measured as 32.3 nW.

3.5. *Characterization of gain control circuit speed and stability*

The accuracy of the detector gain is determined by the stability of the bias voltage. The slope of gain – bias curve is steepest close to the breakdown voltage (Fig. 1(b)), thus variations of gain due to fluctuation of bias voltage will be highest near the breakdown voltage. We confirmed that the fluctuations of bias voltage were less than 0.007 V (Fig. 7(c)), which corresponds to a maximum gain fluctuation of 0.2% at 146 V bias voltage. The overall APD FLIm response speed to a step change of control voltage (5-fold change in APD gain) was less than 2 ms (Fig. 7(d)). No overshoot was observed at either rising or falling edge.

3.6. *Validation on tissue sample*

Figure 8 displays the FLIm parametric map obtained from freehand scanning of the lamb tissue. Areas of bone, bone marrow, fat and muscle are highlighted in the white light image of the tissue sample (Fig. 8(a)). The FLIm point-measurement locations are shown in Figs. 8(b) and (c) for low (120 Hz) and high (480 Hz) laser repetition rate respectively. As expected, better

Optics EXPRESS

FLIm coverage of the tissue sample is achieved with high (480 Hz) laser repetition rate. The augmented FLIm maps from spectral band 470/28 nm for both low (120 Hz) and high (480 Hz) laser repetition rate are shown in Figs. 8(d) and (e). Current results show that distinct tissue type (e.g. bone marrow, bone, fat, muscle) are associated with distinct fluorescence lifetimes and clearly distinguishable from FLIm map. Lifetime values from different tissue types are consistent across FLIm maps of low and high laser repetition rate, indicating good lifetime recovery even with reduced pulse energy. However, a more complete and smoother FLIm map is achieved with higher laser repetition rate despite the reduction in pulse energy.

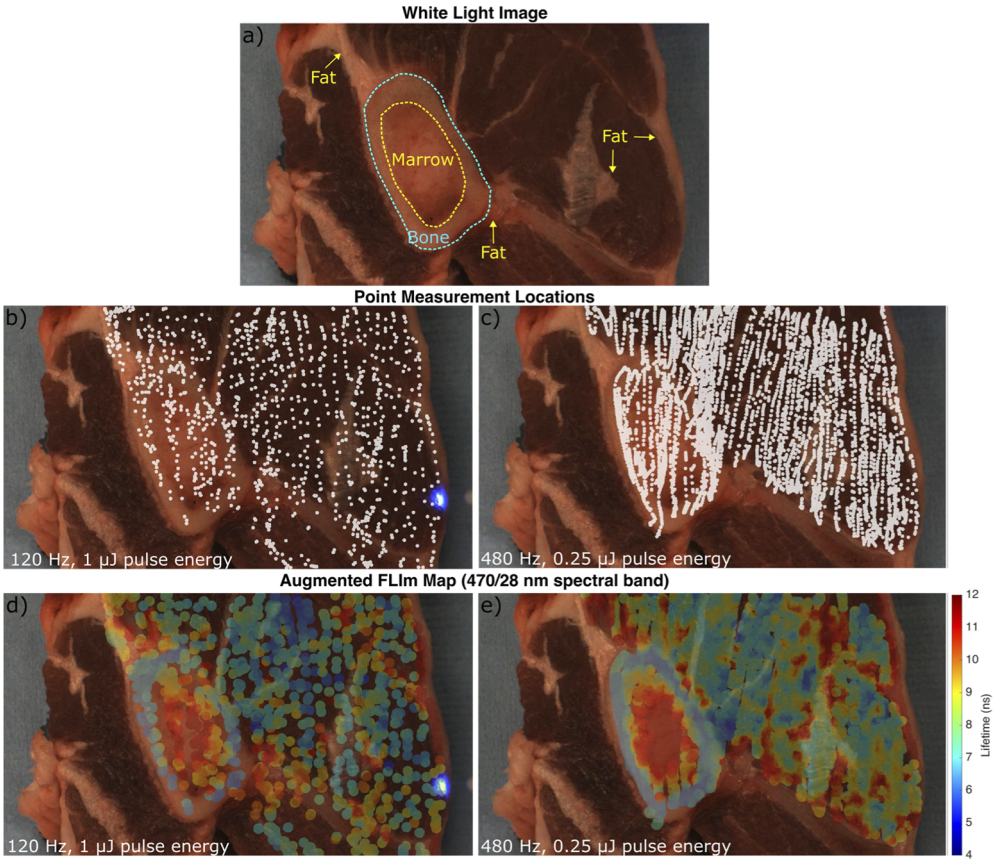

Fig. 8. Representative FLIm images obtained via the freehand scanning of *ex vivo* fresh lamb tissue. a) white light image of lamb tissue sample. b) and c) FLIm points measurement locations for different 355 nm laser configuration. d) and e) white light images of the lamb tissue augmented with lifetime maps from 470/28 nm spectral band under different 355 nm laser repetition rate.

4. Discussion

This study demonstrates the performance of an APD-based FLIm device enabling measurements of fluorophores with a broad range of fluorescence lifetimes (0.5–6.0 ns) simultaneously in multiple emission spectral bands. The instrument is capable of rapid adjustments (< 2 ms) of the detection gain independently for each APD detector resulting in maximization of signal SNR in each spectral channel. Rapid gain adjustment is critical to account for the potential rapid change of fluorescence intensity encountered in clinical setting due to change in probe to

Optics EXPRESS

tissue distance during scanning, differences in quantum efficiencies of endogenous fluorescent molecules and presence of residual blood or other fluids. Moreover, the results show a significant improvement of the signal quality (higher SNR and lower lifetime variability) and imaging speed of the multi-APDs when compared to the previously reported time multiplexing single PMT device.

The ability to recover accurate lifetimes independently from signal intensity levels, detector gain and detector output voltage is of critical importance for fluorescence lifetime measurements. Current results demonstrate that accurate and consistent lifetime values (1% variability of mean lifetime) can be achieved with the multi-APDs FLIm device across a wide range of signal intensity levels (Fig. 6). We observed a broadening of the instrument's IRF at low detector gain and subsequently large lifetime estimation error when a single IRF is used for deconvolution (Fig. 6(b)). Such behavior is expected given the dependance of the terminal capacitance of the APD detector from the detector's gain (reverse bias) [42]. We found that this effect can be addressed by deconvolving the measured signal with an IRF acquired at similar APD gain that resulted in a lifetime accuracy of 1% over the M=8-35 detector gain range (Fig. 6(b)). The small (<0.1 ns) residual error observed at low APD gain (M=4) will be further investigated. For applications where small variation of lifetime are expected, highest accuracy can be achieved by ensuring a gain of no less than 8.

Current results also demonstrate the ability of the prototype multi-APDs FLIm device to accurately resolve fluorescence lifetimes ranging from as short as 0.5 ns to 6.0 ns. This demonstrates that the reduced bandwidth of APD (400 MHz) compared to MCP-PMT (3 GHz) does not prevent the accurate measurement of a fluorophores with a broad range of lifetimes. Comparison of accuracy and precision of lifetime measurement in identical conditions between time multiplexing single PMT FLIm and multi-APDs FLIm demonstrates a 5-fold reduction of lifetime measurement variability in identical conditions. This is due in part to the low integrated noise of APD module (4.06 nW) compared to that of MCP-PMT plus amplifier (32.3 nW). In addition, the high quantum efficiency of APD detector (50% at 400 nm; 75% at 540 nm) compared to that of MCP-PMT (25% at 400 nm; ~9% at 540 nm) also helps improving the SNR of the APD FLIm system. This improvement is particularly relevant for clinical data acquisition, where point measurement rate is currently limited by the maximum permissible exposure of tissue [37]. For example, we demonstrated that FLIm measurements performed in clinical setting at a rate of 30 Hz (1.0 μJ pulse, 120 Hz laser repetition rate, 4-fold average) with the reference MCP system, could be performed as accurately with the proposed system at 120 Hz (0.25 μJ pulse, 480 Hz laser repetition rate, 4 averaging), leading to either a much faster or more complete coverage of the surgical field (Fig. 8). The laser working frequency is limited to 480 Hz for clinical freehand scanning in order to be complied with laser exposure requirements specified by IEC 60825 standard [37]. Specifically, it is determined such that maximum permissible exposure (MPE) would be achieved with a 400 μm-core fiber probe in contact with tissue for 5 seconds of static exposure which is unlikely to happen during freehand scanning. When used with mechanical scanning, point measurement speed of up to 100 kHz (without dynamic gain adjustment) can be easily achieved with the proposed multi-APDs FLIm system. Alternatively, improvements in FLIm detection could be used to better identify small changes in fluorescence lifetime, improving system sensitivity when small lifetime changes are expected such as recellularization of engineered tissue [23]. For applications where measurement speed is not critical, as for some benchtop applications, the proposed system will enable higher resolution imaging by sampling the tissue more densely while reducing data averaging.

FLIm measurements performed with the multi-APDs device reported here will also benefit from the ability to adjust the gain of each individual channel independently. This addresses a limitation of the MCP-PMT based system where the same detector gain is applied across all channels. As a result, the dynamic range of MCP-PMT system is determined by the channel with

Optics EXPRESS

the most signal, thus negatively impacting the SNR of the remaining channels. The APD FLIm system with individual channel gain adjustment capability will improve signal quality for tissue where fluorophores with distinct quantum yield are present in different spectral channels.

Moreover, the small size, low cost and robustness of APD detectors is a clear advantage over MCP-PMT. Independent detectors for each spectral band means that delay fibers are no longer necessary, thus reducing the complexity and cost of the system. In addition, the advance of Si manufacturing technology and integrated circuit design may enable, in the near future, the integration of a microchip laser, multiple APD detectors, their bias control and amplifier circuits as well as a compact multichannel ADC into one integrated circuit board, enabling the fabrication of miniaturized handheld FLIm systems for clinical use.

The APD-based pulse sampling FLIm reported here is well suited for use in clinical settings and compares favorably to most recent developments in TCSPC-based systems. First, it operates at room light with no special accommodation in the operating room lighting conditions, thus making the adoption of the technology straightforward. While TCSPC-based system utilizing synchronous external illumination were recently reported [9,10], implementation in surgical setting would require all light sources to be replaced with sources synchronized with the TCSPC system. Second, the proposed simultaneous multispectral multi-APDs FLIm system can achieve a point measurement rate of 480 Hz, faster than the recently reported data acquisition rate of 50 Hz for the TCSPC based system. This limited acquisition speed stems from the low photon collection efficiency of the reported TCSPC based system due to: the low filling factor (~3%) of the SPAD array, the intrinsic inefficiency of time-gated strategy and the high loss of dispersing optical components. Although these issues could be addressed with additional development, the device reported here provides key benefits to support clinical validation studies of FLIm technology.

The APD-based multispectral FLIm reported here will also facilitate integration of FLIm with other imaging techniques such as Optical Coherence Tomography (OCT) and Ultrasound (US). While multispectral FLIm itself is a powerful imaging tool providing rich tissue biochemical information for disease diagnosis, its utility is greatly enhanced when combined with imaging techniques that provide complementary structural information of tissue such as OCT [43] and US [44]. Integration of FLIm and OCT is particularly advantageous as both modalities can be carried out using a double-clad fiber for full-optical composition and structural imaging endoscopy. The distinct spectral bands of FLIm (355 nm excitation, 400 nm to 700 nm detection) and of OCT (typically 900 nm, 1050 nm or 1310 nm) facilitate the optical integration using dichroic mirrors [45]. The small size of APD detector and simplicity of multi-APDs FLIm instrumentation facilitates the mechanical integration. APD-based FLIm, in combination with a suitable UV light source, enables point measurement rates similar to A-line rates of typical OCT systems (50-100 kHz), thus facilitating future multimodal implementations.

5. Conclusion

We have demonstrated the first APD-based multispectral FLIm system with individual channel gain adjustment capability. Accurate and precise lifetime measurement was achieved across a 10-fold change of excitation intensity and APD gain. In comparison with previously reported multispectral pulse-sampling FLIm systems that rely on temporal multiplexing and a single MCP-PMT, the current design improves the system SNR and allows fast independent dynamic gain adjustment for each optical channel making it better suited for clinical use. Compared to early reported APD based FLIm system [11], the current system offers better responsivity in visible wavelength, multichannel detection for different tissue fluorophores and dynamic gain adjustment capability. The use of low-cost solid-state detectors will facilitate optical and electrical integration and miniaturization, leading to more compact and low-cost fluorescence

Optics EXPRESS

lifetime imaging instrumentation. In addition, the validation plan we developed will serve as a reference for the design, validation, and standardization of future FLIm devices.

Funding. National Institutes of Health (R01CA187427, R01CA250512).

Acknowledgments. The authors also would like to thank Thorlabs, Inc. for technical assistance.

Disclosures. The authors declare no conflicts of interest.

Data availability. Data underlying the results presented in this paper are not publicly available at this time but may be obtained from the authors upon reasonable request.

References

1. M. Y. Berezin and S. Achilefu, "Fluorescence lifetime measurements and biological imaging," Chem. Rev. **110**(5), 2641–2684 (2010).
2. M. Monici, "Cell and tissue autofluorescence research and diagnostic applications," Biotechnol. Annu. Rev. **11**, 227–256 (2005).
3. A. C. Croce and G. Bottiroli, "Autofluorescence spectroscopy and imaging: a tool for biomedical research and diagnosis," Eur. J. Histochem. **58**, 2461 (2014).
4. S. Coda, A. J. Thompson, G. T. Kennedy, K. L. Roche, L. Ayaru, D. S. Bansi, G. W. Stamp, A. V. Thillainayagam, P. M. French, and C. Dunsby, "Fluorescence lifetime spectroscopy of tissue autofluorescence in normal and diseased colon measured ex vivo using a fiber-optic probe," Biomed. Opt. Express **5**(2), 515–538 (2014).
5. B. H. Malik, J. Lee, S. Cheng, R. Cuenca, J. M. Jabbour, Y. S. Cheng, J. M. Wright, B. Ahmed, K. C. Maitland, and J. A. Jo, "Objective Detection of Oral Carcinoma with Multispectral Fluorescence Lifetime Imaging In Vivo," Photochem. Photobiol. **92**(5), 694–701 (2016).
6. J. R. Lakowicz, *Principles of fluorescence spectroscopy* (Springer Science & Business Media, 2013).
7. P. A. De Beule, C. Dunsby, N. P. Galletly, G. W. Stamp, A. C. Chu, U. Anand, P. Anand, C. D. Benham, A. Naylor, and P. M. French, "A hyperspectral fluorescence lifetime probe for skin cancer diagnosis," Rev. Sci. Instrum. **78**(12), 123101 (2007).
8. W. Becker, A. Bergmann, and C. Biskup, "Multispectral fluorescence lifetime imaging by TCSPC," Microsc. Res. Tech. **70**(5), 403–409 (2007).
9. J. L. Lagarto, F. Villa, S. Tisa, F. Zappa, V. Shcheslavskiy, F. S. Pavone, and R. Cicchi, "Real-time multispectral fluorescence lifetime imaging using Single Photon Avalanche Diode arrays," Sci. Rep. **10**(1), 8116 (2020).
10. J. L. Lagarto, V. Shcheslavskiy, F. S. Pavone, and R. Cicchi, "Real-time fiber-based fluorescence lifetime imaging with synchronous external illumination: A new path for clinical translation," J. Biophotonics **13**(3), e201960119 (2020).
11. J. D. Pitts and M.-A. Mycek, "Design and development of a rapid acquisition laser-based fluorometer with simultaneous spectral and temporal resolution," Rev. Sci. Instrum. **72**(7), 3061–3072 (2001).
12. Q. Fang, T. Papaioannou, J. A. Jo, R. Vaitha, K. Shastry, and L. Marcu, "Time-domain laser-induced fluorescence spectroscopy apparatus for clinical diagnostics," Rev. Sci. Instrum. **75**(1), 151–162 (2004).
13. M.-A. Mycek, K. T. Schomacker, and N. S. Nishioka, "Colonic polyp differentiation using time-resolved autofluorescence spectroscopy," Gastrointest Endosc. **48**(4), 390–394 (1998).
14. Y. Sun, R. Liu, D. S. Elson, C. W. Hollars, J. A. Jo, J. Park, Y. Sun, and L. Marcu, "Simultaneous time- and wavelength-resolved fluorescence spectroscopy for near real-time tissue diagnosis," Opt. Lett. **33**(6), 630–632 (2008).
15. D. R. Yankelevich, D. Ma, J. Liu, Y. Sun, Y. Sun, J. Bec, D. S. Elson, and L. Marcu, "Design and evaluation of a device for fast multispectral time-resolved fluorescence spectroscopy and imaging," Rev. Sci. Instrum. **85**(3), 034303 (2014).
16. D. Ma, J. Bec, D. Gorpas, D. Yankelevich, and L. Marcu, "Technique for real-time tissue characterization based on scanning multispectral fluorescence lifetime spectroscopy (ms-TRFS)," Biomed. Opt. Express **6**(3), 987–1002 (2015).
17. D. Gorpas, J. Phipps, J. Bec, D. Ma, S. Dochow, D. Yankelevich, J. Sorger, J. Popp, A. Bewley, R. Gandour-Edwards, L. Marcu, and D. G. Farwell, "Autofluorescence lifetime augmented reality as a means for real-time robotic surgery guidance in human patients," Sci. Rep. **9**(1), 1187 (2019).
18. B. W. Weyers, M. Marsden, T. Sun, J. Bec, A. F. Bewley, R. F. Gandour-Edwards, M. G. Moore, D. G. Farwell, and L. Marcu, "Fluorescence lifetime imaging for intraoperative cancer delineation in transoral robotic surgery," Transl Biophotonics **1**(1-2), e201900017 (2019).
19. A. Alfonso-Garcia, J. Bec, S. Sridharan Weaver, B. Hartl, J. Unger, M. Bobinski, M. Lechpammer, F. Girgis, J. Boggan, and L. Marcu, "Real-time augmented reality for delineation of surgical margins during neurosurgery using autofluorescence lifetime contrast," J. Biophotonics **13**(1), e201900108 (2020).
20. J. Bec, J. E. Phipps, D. Gorpas, D. Ma, H. Fatakdawala, K. B. Margulies, J. A. Southard, and L. Marcu, "In vivo label-free structural and biochemical imaging of coronary arteries using an integrated ultrasound and multispectral fluorescence lifetime catheter system," Sci. Rep. **7**(1), 8960 (2017).
21. X. Zhou, A. K. Haudenschild, B. E. Sherlock, J. C. Hu, J. K. Leach, K. A. Athanasiou, and L. Marcu, "Detection of glycosaminoglycan loss in articular cartilage by fluorescence lifetime imaging," J Biomed Opt **23**(12), 1–8 (2018).

Optics EXPRESS

22. J. E. Phipps, D. Gorpas, J. Unger, M. Darrow, R. J. Bold, and L. Marcu, "Automated detection of breast cancer in resected specimens with fluorescence lifetime imaging," Phys Med Biol **63**(1), 015003 (2017).
23. A. Alfonso-Garcia, J. Shklover, B. E. Sherlock, A. Panitch, L. G. Griffiths, and L. Marcu, "Fiber-based fluorescence lifetime imaging of recellularization processes on vascular tissue constructs," J. Biophotonics **11**(9), e201700391 (2018).
24. A. K. Haudenschild, B. E. Sherlock, X. Zhou, J. C. Hu, J. K. Leach, L. Marcu, and K. A. Athanasiou, "Non-destructive detection of matrix stabilization correlates with enhanced mechanical properties of self-assembled articular cartilage," J Tissue Eng Regen Med **13**(4), 637–648 (2019).
25. S. Shrestha, B. E. Applegate, J. Park, X. Xiao, P. Pande, and J. A. Jo, "High-speed multispectral fluorescence lifetime imaging implementation for in vivo applications," Opt Lett **35**(15), 2558–2560 (2010).
26. D. S. Kittle, F. Vasefi, C. G. Patil, A. Mamelak, K. L. Black, and P. V. Butte, "Real time optical Biopsy: Time-resolved Fluorescence Spectroscopy instrumentation and validation," Sci. Rep. **6**(1), 38190 (2016).
27. H. S. Nam, W. J. Kang, M. W. Lee, J. W. Song, J. W. Kim, W. Y. Oh, and H. Yoo, "Multispectral analog-mean-delay fluorescence lifetime imaging combined with optical coherence tomography," Biomed. Opt. Express **9**(4), 1930–1947 (2018).
28. S. Cheng, R. M. Cuenca, B. Liu, B. H. Malik, J. M. Jabbour, K. C. Maitland, J. Wright, Y. S. Cheng, and J. A. Jo, "Handheld multispectral fluorescence lifetime imaging system for in vivo applications," Biomed. Opt. Express **5**(3), 921–931 (2014).
29. R. A. Romano, R. G. Teixeira Rosa, A. G. Salvio, J. A. Jo, and C. Kurachi, "Multispectral autofluorescence dermoscope for skin lesion assessment," Photodiagnosis Photodyn Ther **30**, 101704 (2020).
30. M. Marsden, T. Fukazawa, Y. C. Deng, B. W. Weyers, J. Bec, D. Gregory Farwell, and L. Marcu, "FLImBrush: dynamic visualization of intraoperative free-hand fiber-based fluorescence lifetime imaging," Biomed. Opt. Express **11**(9), 5166–5180 (2020).
31. V. Mackowiak, J. Peupelmann, Y. Ma, and A. Gorges, "NEP–noise equivalent power," *Thorlabs, Inc* (2015).
32. J. Kim, M. Lee, J.-H. Yang, and J.-H. Choy, "Photophysical Properties of Hemicyanine Dyes Intercalated in Na−Fluorine Mica," The Journal of Physical Chemistry A **104**(7), 1388–1392 (2000).
33. L. Rabiner, R. Schafer, and D. Dlugos, "Programs for Digital Signal Processing," edited by *Digital Signal Processing Committee of the IEEE Acoustics, Speech and Signal Processing Society* (IEEE, 1979).
34. T. J. Paulus, "Timing Electronics and Fast Timing Methods with Scintillation Detectors," Ieee T Nucl Sci **32**(3), 1242–1249 (1985).
35. D. A. Gedcke and W. J. McDonald, "A constant fraction of pulse height trigger for optimum time resolution," Nuclear Instruments and Methods **55**, 377–380 (1967).
36. J. Liu, Y. Sun, J. Y. Qi, and L. Marcu, "A novel method for fast and robust estimation of fluorescence decay dynamics using constrained least-squares deconvolution with Laguerre expansion," Physics in Medicine and Biology **57**(4), 843–865 (2012).
37. International Electrotechnical Commission, "Safety of Laser Products - Part 1: Equipment Classification, and Requirements," IEC 60825–1 (2014).
38. H. Pal, S. Nad, and M. Kumbhakar, "Photophysical properties of coumarin-120: Unusual behavior in nonpolar solvents," The Journal of Chemical Physics **119**(1), 443–452 (2003).
39. D. Magde, G. E. Rojas, and P. G. Seybold, "Solvent Dependence of the Fluorescence Lifetimes of Xanthene Dyes," Photochem. Photobiol. **70**(5), 737–744 (1999).
40. A. S. Dabir, C. A. Trivedi, Y. Ryu, P. Pande, and J. A. Jo, "Fully automated deconvolution method for on-line analysis of time-resolved fluorescence spectroscopy data based on an iterative Laguerre expansion technique," J Biomed Opt **14**(2), 024030 (2009).
41. A. Žukauskas, P. Vitta, N. Kurilčik, S. Juršėnas, and E. Bakienė, "Characterization of biological materials by frequency-domain fluorescence lifetime measurements using ultraviolet light-emitting diodes," Opt Mater **30**(5), 800–805 (2008).
42. B. Steindl, R. Enne, S. Schidl, and H. Zimmermann, "Linear Mode Avalanche Photodiode With High Responsivity Integrated in High-Voltage CMOS," Ieee Electr Device L **35**(9), 897–899 (2014).
43. M. W. Lee, J. W. Song, W. J. Kang, H. S. Nam, T. S. Kim, S. Kim, W. Y. Oh, J. W. Kim, and H. Yoo, "Comprehensive intravascular imaging of atherosclerotic plaque in vivo using optical coherence tomography and fluorescence lifetime imaging," Sci. Rep. **8**(1), 14561 (2018).
44. H. Fatakdawala, D. Gorpas, J. W. Bishop, J. Bec, D. Ma, J. A. Southard, K. B. Margulies, and L. Marcu, "Fluorescence Lifetime Imaging Combined with Conventional Intravascular Ultrasound for Enhanced Assessment of Atherosclerotic Plaques: an Ex Vivo Study in Human Coronary Arteries," J Cardiovasc Transl Res **8**(4), 253–263 (2015).
45. B. E. Sherlock, J. E. Phipps, J. Bec, and L. Marcu, "Simultaneous, label-free, multispectral fluorescence lifetime imaging and optical coherence tomography using a double-clad fiber," Opt Lett **42**(19), 3753–3756 (2017).